INSTITUTE OF PHYSICS PUBLISHING JOURNAL OF NEURAL ENGINEERING

J. Neural Eng. **3** (2006) 306–315 doi:10.1088/1741-2560/3/4/008

Bio-heat transfer model of deep brain stimulation-induced temperature changes

Maged M Elwassif, Qingjun Kong, Maribel Vazquez and Marom Bikson[1]

Department of Biomedical Engineering, The City College of New York of The City University of New York, NY, USA

E-mail: bikson@ccny.cuny.edu

Received 10 April 2006
Accepted for publication 12 October 2006
Published 6 November 2006
Online at stacks.iop.org/JNE/3/306

Abstract

There is a growing interest in the use of chronic deep brain stimulation (DBS) for the treatment of medically refractory movement disorders and other neurological and psychiatric conditions. Fundamental questions remain about the physiologic effects of DBS. Previous basic research studies have focused on the direct polarization of neuronal membranes by electrical stimulation. The goal of this paper is to provide information on the thermal effects of DBS using finite element models to investigate the magnitude and spatial distribution of DBS-induced temperature changes. The parameters investigated include stimulation waveform, lead selection, brain tissue electrical and thermal conductivities, blood perfusion, metabolic heat generation during the stimulation and lead thermal conductivity/heat dissipation through the electrode. Our results show that clinical DBS protocols will increase the temperature of surrounding tissue by up to 0.8 °C depending on stimulation/tissue parameters.

(Some figures in this article are in colour only in the electronic version)

Introduction

The electrical stimulation of tissues can lead to temperature increases as a result of both Joule heat and metabolic responses to stimulation [1–3, 5, 6]. Electrical stimulation-induced changes in temperature can profoundly affect tissue function; moderate temperature increases are not necessarily necrotic. The role of temperature increases during clinical deep brain stimulation (DBS) has not been previously considered.

Joule heat will be produced in any electrical field, where electrical currents are circulating [36]. The magnitude and spatial distribution of the induced temperature changes are a function of tissue properties and electrical stimulation parameters. Electrical stimulation has been used as a tool to analyze brain metabolism and related temperature increases [4–7]. Numerical models of radio-frequency ablation probes show that voltage greater than 10 V_{rms} will increase temperature to 40 °C or more [2, 3]. These reports indicate that reducing stimulation intensity reduces peak temperature increases, but did not explicitly examine stimulation voltages sufficient to induce moderate (<2 °C) temperature changes. Electrical stimulation in rat brains with micro-electrodes (1–10 s, 0.5 ms pulse duration, 10–20 Hz, at stimulation intensities below those generating seizures) has been shown to increase brain temperature up to 0.1–0.5 °C, 1 mm from the stimulating electrodes [5, 6].

Brain function is especially sensitive to the changes in temperature. An increase in temperature by ∼1 °C can have profound effects on a single neuron and neuronal network function [8–12]. For most membrane channels, the temperature dependence of conductance is comparable to that of a diffusion-limited process, while the temperature dependence of channel gating and pump kinetics can exceed this value by more than an order of magnitude [11, 14]. All biophysical properties, including those suggested to play a role in the effects of DBS, are temperature dependent. These include membrane properties such as passive resistance/capacitance and voltage-gated channel kinetics. Changes in membrane properties will affect firing threshold, peak firing

[1] Current address: Department of Biomedical Engineering, The City College of New York, 140th street and Convent Avenue, T-403B, Steinman Hall, NY 10031, USA.

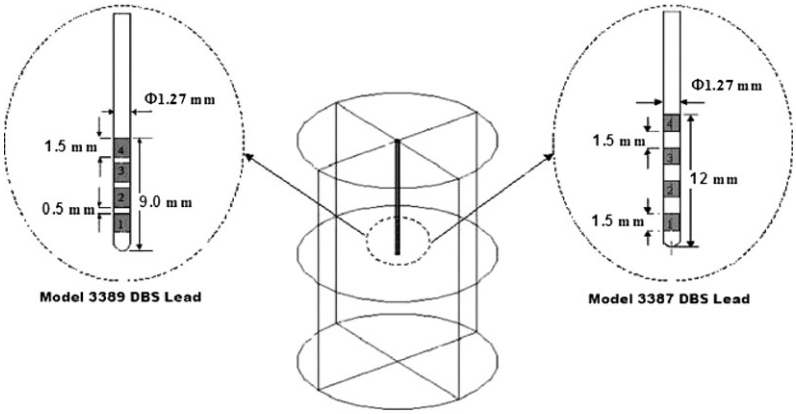

Figure 1. Schematic diagram of model geometrical configuration. We modeled the brain tissue as a cylinder, 5 cm radius and 14 cm height. The bottom (distal end) of the DBS lead was positioned at the center of the tissue (center). Two DBS leads were modeled: the 3389 DBS lead with 1.5 mm electrodes and 0.5 mm spacing between electrodes (left) and the 3387 DBS lead with 1.5 mm electrodes and 1.5 spacing (right). The electrode index used is indicated.

rate [28] and depolarization block threshold in response to DBS [37]. Excitatory and/or inhibitory synaptic transmission has been suggested to mediate the effects of DBS [14]; both are highly sensitive to temperature changes [8, 10, 12, 15]. Temperature-dependent changes in pump kinetics will affect the regulation of the neuronal environment including the accumulation of neurotransmitters and ions. Extracellular potassium accumulation, which is associated with high-frequency electrical stimulation and has been suggested to play a role in DBS [16, 17], is highly sensitive to temperature changes and related metabolic activity [18, 19]. Research on the mechanisms of DBS has also focused on associated neurotransmitter concentration changes [20–24] whose release and clearance kinetics will both change with temperature. Potential DBS-induced changes in brain temperature are thus of broad interest in quantifying the mechanisms of DBS.

Besides Joule heat, DBS may further increase brain temperature through increasing neuronal activity and concomitant metabolic activity, e.g. ion/neurotransmitter pumps [6, 7, 25, 49]. Indeed, DBS is generally associated with a local increase in metabolic activity [26–28]. Both tissue heating and increased metabolic activity may promote increased blood flow as is observed during DBS [43].

The range of physiological (non-necrotic) temperature transients, for example in response to sensory stimuli, remains unclear; changes up to 2 to 3 °C have been reported [6, 8, 49]. Thus, moderate (<2 °C) changes in brain temperature, induced by deep brain stimulation, may exert a profound effect on neuronal function without leading to cell damage.

It is beyond the scope of this study to fully dissect the complex effects of any temperature changes on overall neuronal function and DBS safety/efficacy. However, determining the magnitude and spatial distribution of induced temperature changes is a first step in understanding the role of heating in DBS. In this paper, we used finite element models to investigate how biological properties and DBS stimulation parameters affect the magnitude and spatial distribution of the DBS-induced temperature field. By solving the coupled Laplace equation of electrical field and the Pennes bio-heat transfer equation, we are able to simulate how DBS affects the temperature field distribution in brain tissue.

Model methods

General description

We developed a bio-heat transfer model for DBS using FEMLAB 3.2 (COMSOL Inc., Burlington, MA) implementing the Pennes model. We studied two types of Medtronic leads (figure 1), the Model 3387 DBS lead, with a 1.5 mm spacing between each of the four electrodes at a distal end to provide an electrodes spread over a total of 10.5 mm and the Model 3389 DBS lead, with a 0.5 mm spacing between each of the four electrodes to provide an electrode spread over a total of 7.5 mm. (Medtronic, Inc., MN). We used direct matrix inversion (UMFPACK solver) with 20 296 elements, doubling the resolution-modulated temperature changes by <0.05 °C.

Finite element analysis was used to analyze the effect of DBS on temperature increases in brain tissue. Because of axial geometrical symmetry, the temperature and electrical fields were assumed to vary only with the direction of r, coordinate of radius of the stimulator, and z, coordinate of length of the stimulator. The three-dimensional transfer model geometry can thus be mathematically implemented in two dimensions.

We examined DBS-induced temperature increases in three increasingly detailed situations.

Case 1. Temperature distribution induced by DBS in homogenous brain tissue without blood perfusion or metabolic activity.

Case 2. Temperature distribution induced by DBS in homogenous brain tissue with blood perfusion (solved using the two-dimensional Pennes model) with and without related metabolic activity.

Case 3. Temperature distribution induced by DBS in non-homogenous brain tissue with consideration of physical properties of the DBS leads and tissue damage around the electrode.

In each of the above cases, we determined the range of temperature increases expected *in vivo* by parameter sensitivity analysis.

Methods and analysis

Blood perfusion occurs in living tissues, and the passage of blood modifies the heat transfer in tissues. Furthermore, metabolic activity generates heat within the tissue. Pennes (1948) and Perl (1962) have established a simplified bio-heat transfer model to describe heat transfer in tissue by considering the effects of blood perfusion and metabolism [30]. During electrical stimulation (DBS), additional Joule heating arises when energy dissipated by an electric current flowing through a conductor is converted into thermal energy. The resulting bio-heat equation (1) governs heating during electrical stimulation [1, 3, 42]:

$$\rho C_{\mathrm{p}} \frac{\partial T}{\partial t} = \nabla(k\nabla T) - \rho_{\mathrm{b}}\omega_{\mathrm{b}}C_{\mathrm{b}}(T - T_{\mathrm{b}}) + Q_{\mathrm{m}} + \sigma|\nabla V|^2, \tag{1}$$

where ρ_{b} is the blood density (kg m^{-3}), C_{b} is the heat capacity of the blood (J kg^{-1} °C^{-1}), k is the thermal conductivity of the brain tissue (W m^{-1} °C^{-1}), T is the temperature (°C), ω_{b} is the blood perfusion (ml s^{-1} cm^{-3}), ρ is the brain tissue density, T_{b} is the body core temperature (°C) and Q_{m} is the metabolic heat source term (W m^{-3}). In this report, consideration of only steady-state temperature increases is consistent with continuous (chronic) deep brain stimulation and our interest determining maximum temperature increases (preliminary stimulations indicate that steady-state temperature is reached in less than 15 min). We modeled the Joule heat induced by DBS stimulation with a source term $\sigma|\nabla V|^2$, where σ is the electrical conductivity of the tissue and V is the electrical potential induced by stimulation. The electrical potential was determined by solving the Laplace equation $\nabla \cdot (\sigma \nabla V) = 0$. We modeled a constant voltage between the electrodes calculated from the root-mean-squared (rms) voltage of the DBS stimulation (equation (2)); the DBS waveforms were based on direct measurements from the actual stimulator and were biphasic and charge balanced with a cathodic pulse equal to the user-defined pulse width followed by an anodic recharge pulse. The anodic pulse begins 0.4 ms after the end of the cathodic pulse and ends ∼4 ms before the beginning of the next cathodic pulse:

$$V_{\mathrm{rms}} = \sqrt{1/T_{\mathrm{p}} \int_0^{T_{\mathrm{p}}} v(t)^2 \, \mathrm{d}t}, \tag{2}$$

where T_{p} is the pulse period.

We evaluated two normal DBS electrical settings: 'high setting' (10 V, 185 pps, 210 ms) with V_{rms} of 1.561 volts and 'typical setting' (3 V, 185 pps, 90 ms) with V_{rms} of 0.353 volts [31]. Because stimulation using the typical setting never resulted in temperature increases greater than 0.3 °C, our results focus on the more temperature-significant high setting.

The following range of tissue and lead parameters was applied.

Biological properties of the brain tissue [3, 29, 32–34]:
κ_{t}: thermal conductivity of the brain tissue (W m^{-1} °C^{-1}) = 0.45–0.6,
ρ_{b}: density of the brain tissue (kg m^{-3}) = 1040,
C_{p}: specific heat of the brain tissue (J kg^{-1} °C^{-1}) = 3650,
σ: electrical conductivity (S m^{-1}) = 0.15–0.35,
T_{i}: initial temperature of the brain tissue = 37 °C.

Biological properties of the blood [33, 34]:
ω_{b}: volumetric blood perfusion rate per unit volume (ml s^{-1} cm^{-3}) = 0.004–0.012,
ρ_{b}: density of the blood (kg m^{-3}) = 1057,
C_{b}: specific heat of the blood (J kg^{-1} °C^{-1}) = 3600,
T_{b}: body core temperature = 36.7 °C.

Physical properties of the DBS lead materials:
for the insulation portion of the leads (80 A urethane) [38, 40, 41]:
κ_{i} (W m^{-1} °C^{-1}) = 0.026, ρ_{i} (kg m^{-3}) = 1110, C_{i} (J kg^{-1} °C^{-1}) = 1500, σ_{i} (S m^{-1}) = 10^{-10};

for the electrode portion of the leads (platinum/iridium: Pt 90/Ir 10) [39–41]:
κ_{e} (W m^{-1} °C^{-1}) = 31, ρ_{e} (kg m^{-3}) = 21 560, C_{e} (J kg^{-1} °C^{-1}) = 134, σ_{e} (S m^{-1}) = 4×10^6.

Dimensions and boundary conditions. In order to obtain the particular solutions to the coupling temperature and electrical field, boundary conditions and initial conditions were required. The dimensions of the brain tissue that we modeled in FEMLAB must be appropriately chosen to be large enough to abate boundary effects on temperature and electrical distribution close to the lead surface as well as small enough to allow for a reasonable computational time. In our model, the geometry of the brain tissue was set as a cylinder with radius 50 mm and height 140 mm, as shown in figure 1. For the boundary conditions of the electrical field, the voltage between the two energized electrodes, either 1 and 4 (figures 2(A) and (C)) or 1 and 2 (figures 2(B) and (D)), was set to V_{rms}. The outer boundaries of the brain tissue were treated as electrically insulated, namely $\partial V/\partial n = 0$. For the thermal boundary conditions, the temperature at the outer boundaries of the brain tissue was fixed at 37 °C [29, 34]; this assumption is valid if (1) there are no ambient temperature (convective) gradients across deep brain structures [33] and (2) there is no DBS-induced heating at the model boundaries (model dimensions). In this paper, we did not consider the effect of cystic cavities containing cerebrospinal fluid (CSF) on the electrical field profile [53] or explicitly consider the CSF convection.

Results

Temperature distribution induced by DBS in homogenous brain tissue without blood perfusion or metabolic activity

In our first iteration (case 1), we focused on how the temperature increased solely in response to DBS-induced Joule heat, without modeling the contribution of blood

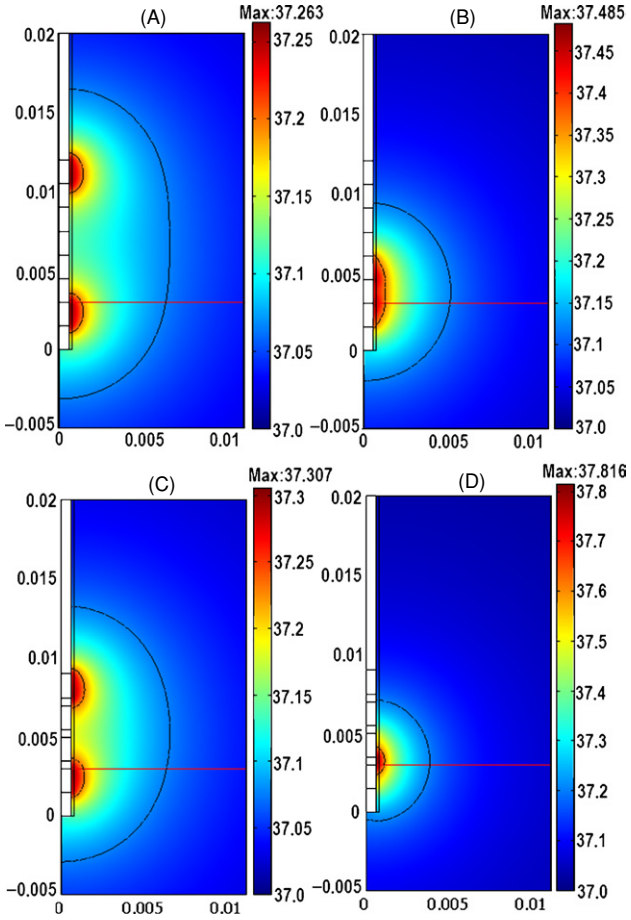

Figure 2. Bio-heat transfer model of deep brain stimulation: effects of lead and electrode selection. The false color maps indicate the spatial temperature distribution around the bipolar stimulating electrodes, when the high stimulation setting was applied, in a homogenous brain with tissue electrical conductivity $\sigma = 0.35$ S m^{-1}, tissue thermal conductivity $\kappa_t = 0.527$ W m^{-1} °C^{-1} and no blood perfusion. The red 'axial' line is the cross section at the proximal end of the most distal electrode (at height $z = 3$ mm) extending in the r direction from the electrode; in the remaining figures the temperature profile is plotted along this line. (A) Lead 3387, the first and fourth electrodes were electrically conductive. (B) Lead 3387, the first and second electrodes were electrically conductive. (C) Lead 3389, the first and fourth electrodes were electrically conductive. (D) Lead 3389, the first and second electrodes were electrically conductive.

perfusion or metabolic activity. Therefore, in this section, both ω_b and Q_m are zero. This model also treated the DBS electrode shaft to be electrically and thermally insulated, except that electrodes 1 and 2 (the two electrodes most distal on the DBS lead) were electrically energized.

We modeled the temperature distributions using two types of DBS leads, Medtronic DBS Lead 3387 and Lead 3389. We applied 'high setting' to the two DBS leads and investigated how electrical conductivity and thermal conductivity affected the resulting temperature distribution in the brain tissue. Figure 3(A) and table 1-I show changes in peak temperature and temperature field distribution as a function of tissue electrical conductivity ($\sigma = 0.15$–0.35 S m^{-1}) with thermal

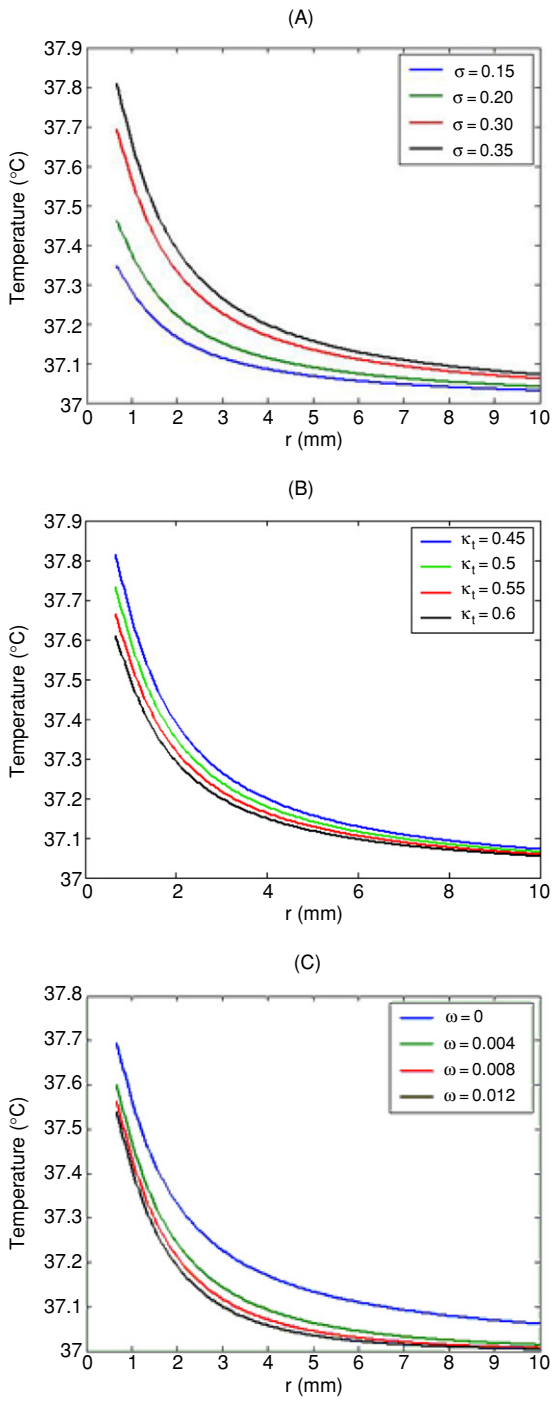

Figure 3. Temperature distribution along the axial direction when the high stimulation setting (Lead 3389, electrodes 1 and 2) was applied in a homogenous brain. (A) Temperature versus electrical conductivity (σ); the thermal conductivity κ_t was fixed at 0.527 W m^{-1} °C^{-1} and blood perfusion was absent. Tissue temperature increased with increasing electrical conductivity. (B) Temperature versus thermal conductivity; the electrical conductivity was fixed at 0.3 S m^{-1} and blood perfusion was absent. Tissue temperature decreased with increasing thermal conductivity κ_t. (C) Temperature distribution versus blood perfusion; electrical conductivity and thermal conductivity were constant (0.30 S m^{-1} and 0.527 W m^{-1} °C^{-1}). Blood temperature was 37°C and metabolic heats were absent.

Table 1. The effects of biological parameters on peak temperature induced by deep brain stimulation. (high setting, electrodes 1 and 2 were energized).

	Electrical conductivity σ (S m^{-1})	Thermal conductivity κ_t (W m^{-1} °C^{-1})	Blood perfusion ω_b (ml s^{-1} cm^{-3})	Peak temperature (°C)	
				3389 DBS lead	3387 DBS lead
I	0.15			37.35	37.21
	0.20			37.47	37.28
	0.30	0.527	0	37.70	37.42
	0.35			37.82	37.48
II		0.45		37.82	37.48
		0.50		37.74	37.44
	0.30	0.55	0	37.67	37.40
		0.60		37.62	37.37
III			0	37.70	37.42
			0.004	37.61	37.34
	0.30	0.527	0.008	37.57	37.31
			0.012	37.54	37.29

Table 2. Peak temperature versus insulation lead thermal conductivity (κ_i) at setting $\sigma = 0.3$ S m^{-1}, $\kappa_t = 0.527$ W m^{-1} °C^{-1} with no blood perfusion and metabolic heat. High stimulation setting was applied to various combinations of leads and energized electrodes.

	3389 DBS lead T_{max} (°C)		3387 DBS lead T_{max} (°C)	
κ_i (W m^{-1} °C^{-1})	Electrodes 1 and 4	Electrodes 1 and 2	Electrodes 1 and 4	Electrodes 1 and 2
0.026	37.26	37.58	37.22	37.37
1	37.24	37.5	37.20	37.35
5	37.22	37.43	37.18	37.31
10	37.21	37.40	37.17	37.29
20	37.20	37.38	37.16	37.27

conductivity (κ_t) fixed at 0.527 W m^{-1} °C^{-1}. Figure 3(B) and table 1-II show changes in peak temperature and temperature field distribution as a function of tissue thermal conductivity (0.45–0.60 W m^{-1} °C^{-1}) with tissue electrical conductivity fixed at 0.3 S m^{-1}. Our results show that temperature increases with electrical conductivity while temperature decreases as thermal conductivity increases. The peak temperature on the lead's surface increased by 0.48 °C at $\sigma = 0.45$ S m^{-1} and $\kappa_t = 0.30$ W m^{-1} °C^{-1} for Lead 3387 and 0.82 °C for Lead 3389 (table 1-I). The temperature field distribution using Lead 3387 was similar to that using Lead 3389. The temperature field space constant defined here as the radial distance from the electrode where the temperature field decreased to 75% (first contour line in figure 2) of its peak value (at the electrode surface) was not affected by changing homogenous tissue electrical or thermal conductivity (appendix A).

Across tissue parameters, the peak temperature for Lead 3389 was approximately 0.3 °C higher than that for Lead 3387 (table 1); this difference can be attributed to the increased distance between Lead 3387 electrodes (figure 2). Similarly, for either Lead 3389 or Lead 3387, changing lead selection such that the leads where farther apart (e.g. leads 1 and 4) significantly reduced peak temperature increases (table 2).

Temperature distribution induced by DBS in homogenous brain tissue with blood perfusion and no metabolic activity

To study how the convection of blood regulates brain temperature during DBS, the blood perfusion rate, ω_b, varied in our model from 0 to 0.012 ml s^{-1} cm^{-3}. In order to isolate how blood perfusion affected the temperature distribution, metabolic activity was not considered in this iteration of the model and blood temperature was fixed at 37 °C. In this section (case 2, without metabolic heat), the electrical conductivity and thermal conductivity were fixed at 0.30 S m^{-1} and 0.527 W m^{-1} °C^{-1}, respectively, and we evaluated only the high setting on DBS electrodes 1 and 2. As shown above, the temperature increased to 37.42 °C and 37.7 °C with the lead models 3387 and 3389 under these conditions without blood perfusion (table 1-I). The addition of blood perfusion convected Joule heat out of the brain tissue so that the peak temperature decreased by increasing the blood perfusion (figure 3(C)). The peak temperature decreased moderately by 0.08 °C and 0.13 °C for Lead 3387 when the blood perfusion rates were 0.004 ml s^{-1} cm^{-3} and 0.012 ml s^{-1} cm^{-3}, respectively (table 1-III)). Similarly, decreases by 0.09 °C and 0.16 °C occurred in the case using Lead 3389 when the blood perfusion rates were 0.004 ml s^{-1} cm^{-3} and 0.012 ml s^{-1} cm^{-3}, respectively. In contrast to the effects of changing tissue electrical/thermal conductivity, changes in blood perfusion rate affected the brain temperature space constant; an increasing perfusion rate decreased the space constant (i.e. the temperature decreased over the distance at a faster rate).

Effects of blood perfusion and metabolic heat on temperature distribution induced by DBS in a homogenous brain.

Metabolic activity, due to baseline brain metabolism and increased metabolism in response to DBS, will act as a heat source inside the brain. Normally, blood perfusion regulates the brain temperature by convecting metabolic heat away. In this section (case 2, with metabolic heat), we considered the temperature of blood circulating in the brain tissue as 36.7 °C [34], 0.3 °C lower than the initial brain temperature. In this

section, we investigated how the interaction between metabolic heat generation and blood perfusion-modulated DBS-induced temperature increases. Prior to application of DBS, we balanced the various metabolic rates with blood perfusion rates such that the baseline brain temperature remained at 37 °C. The metabolic heat required to balance the initial brain temperature was calculated from $Q_m = C_b \rho_b \omega_b (T - T_b)$; for blood perfusion values of 0.004, 0.008 and 0.012 ml s^{-1} cm^{-3}, we applied metabolic heat Q_m of 4566, 9132 and 13 698 W m^{-3}, respectively (interestingly these calculated metabolic rates closely approximate measured values; [29, 33, 34]).

Using these three initial settings (combination of balanced metabolic and perfusion rates), we studied the temperature increases (from 37 °C) due to DBS. Temperature profiles were exactly the same as those in the study considering blood perfusion (at 37 °C) *without* metabolic activity; this was mathematically expected given the equality between metabolism and perfusion set above. As noted above, these temperature profiles were lower than those without metabolic heat and without blood perfusion; this can be explained by the increased blood flow capacity to *both* balance the metabolic heat and reduce the Joule heat.

Temperature distribution induced by DBS considering the inhomogenous physical properties of the DBS lead with and without a tissue encapsulation layer

In this section (case 3), the thermal and electrical properties of the DBS leads were explicitly considered (previously, the DBS leads were modeled as electrically and thermally perfectly insulated). We fixed the thermal conductivity, $\kappa_e = 31$ W m^{-1} $°C^{-1}$, and electrical conductivity, $\sigma_e = 4 \times 10^6$ S m^{-1}, of the DBS platinum/iridium electrodes. We considered the thermal conductivity of the Medtronic DBS lead insulation material (urethane), present everywhere except the electrodes, as 0.026 W m^{-1} $°C^{-1}$. In our simulations, we also considered a range of potential insulation material thermal conductivities (κ_i) from 0.026 W m^{-1} $°C^{-1}$ to 20 W m^{-1} $°C^{-1}$ in order to evaluate the effects of substitute insulation materials on DBS-induced temperature increases. Figure 4(A) shows the temperature distribution over the distance for different lead insulation thermal conductivity values (κ_i), using the high stimulation setting, without blood perfusion and metabolic heat, and tissue thermal and electrical conductivity fixed at $\kappa_t = 0.527$ W m^{-1} $°C^{-1}$ and $s = 0.3$ S m^{-1}, respectively. Table 2 shows that the peak tissue temperature decreased by 0.1–0.2 °C as a result of considering lead properties; the insulation thermal conductivity (κ_i) acts as a heat sink. Figures 4(A) and (B) illustrate how the insulation segments of the electrode could act as a heat sink; the temperature was convected inside the lead insulation and reduced the heat from the tissue.

A sheath of encapsulation tissue around DBS leads may form due to mechanical damage to the brain tissue during lead implantation; the electrical conductivity and width of the encapsulation tissue were previously estimated as $\sigma_{dt} = 0.15$ S m^{-1} and 0.4 mm thick, respectively [35]. We treated the thermal conductivity of the encapsulation tissue as equal to that

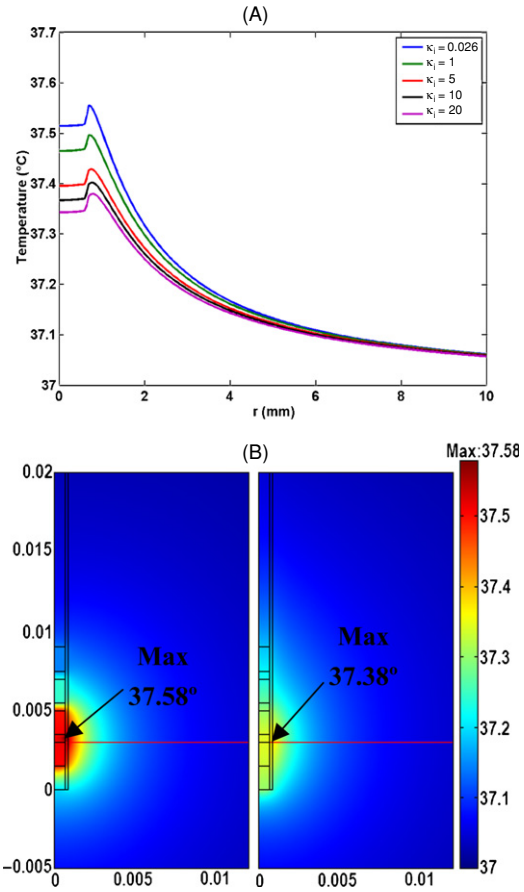

Figure 4. Temperature distribution in a non-homogenous medium along the axial direction when the high stimulation setting (electrodes 1 and 2) was applied. Metabolic heat and blood perfusion were absent. (A) Temperature versus lead insulation thermal conductivity. Increasing the lead insulation thermal conductivity decreased the temperature around the electrode. (B) Temperature field in the 3389 DBS lead and surrounding brain tissue with the lead insulation thermal conductivity (κ_i) equal to 0.026 W m^{-1} $°C^{-1}$ (left) and equal to 20 W m^{-1} $°C^{-1}$ (right). A false color map indicates the spatial temperature distribution around the electrodes. The red line is the 'axial' cross section represented in other figures.

of the brain tissue, i.e. $\kappa_t = 0.527$ W m^{-1} $°C^{-1}$. We simulated how this encapsulation tissue affected the DBS-induced temperature increases; we considered tissue conditions and included the properties of the DBS lead. The addition of an encapsulation layer in our model slightly reduced the peak temperature increase at the electrode surface (now inside the encapsulation layer) by 0.07–0.18 °C, depending on the lead model and electrode configuration tested.

Discussion

Our results, using a reduced model, predict that clinical DBS protocols can induce temperature increases up to 1 °C in the surrounding brain tissue; the peak magnitude of these changes and their spatial distribution depend on a combination of stimulation settings, electrode physical properties and tissue

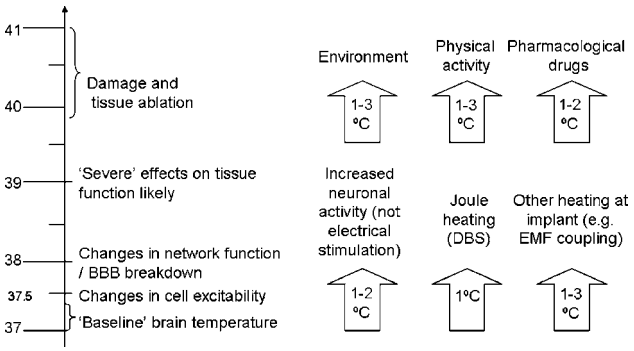

Figure 5. Summary of tissue responses to temperature increases (left) due to multiple heating factors (right). The brain is sensitive to small temperature changes. Changes in cell excitability are evident for temperature changes of 0.5 °C, and changes in network function and blood–brain barrier function are evident for 1 °C increases [49, 51, 58]. A sustained increase to 39 °C can have profound effects on brain function [49], and cell damage/tissue ablation is observed at sustained temperature over 40 °C (just 3 °C over ambient temperature levels). Brain temperature near implants can increase as a result of normal device function (e.g. battery use) or unexpected effects (e.g. EMF coupling with an implant [59, 60]) as well as a result of electrical stimulation (Joule heating and concomitant increased metabolic activity). Though the brain's temperature is regulated, it is not insensitive to environmental temperature increase; these will be compounded during physical activity [49, 57]. Temperature increases result from (normal) neuronal activation associated with behavioral conditions (stress, emotional, sexual behavior, sensory processing [49, 55, 56]). Finally, pharmacological drugs can significantly increase the brain temperature [49]. The above heating factors may be concurrent and thus cumulative (though not necessarily in a linear fashion).

properties. The sensitivity of the brain to small temperature fluctuations, in particular when considering concurrent heating factors, is summarized in figure 5. The precise magnitude and spatial distribution of temperature changes will determine the relevance of these changes to understanding the mechanisms of DBS. It is important to emphasize that the DBS-induced temperature increase is not proposed as a substitute for existing mechanisms of DBS action, but as complimentary and critical for a quantitative prediction of the DBS effects.

For the high stimulation setting, peak temperature increases from 0.2–0.8 °C were predicted in a homogenous medium depending on lead selection and tissue properties (including balanced baseline metabolic and blood perfusion, but neglecting DBS-induced imbalances). The inhomogeneities considered, including a potential encapsulation layer and actual lead physical properties, can decrease peak temperature increases by ∼0.1–0.2 °C.

Effects of DBS lead selection and stimulation settings on brain temperature increases

For the high stimulation setting and using electrodes 1 and 2, the temperature increase using Lead 3387 was roughly 0.2 °C lower than that using Lead 3389 across different lead/tissue properties; this was because Lead 3387 had a larger spacing distance between adjacent electrodes than Lead 3389. For similar reasons, for both lead types, the peak temperature increase is highly dependent on energized electrode selection. The degree of interaction between the electrodes will depend on tissue and lead material properties.

Increasing stimulation intensity, by increasing pulse frequency, duration or amplitude, will increase the Joule heat generation, and hence brain temperature increases. It should be noted that doubling stimulation frequency or pulse duration will double the rms value of stimulation, while doubling stimulation amplitude will quadruple the rms. In addition, the peak temperature does not necessarily increase linearly with the rms value of stimulation. The results of the present study provide an initial basis for determining DBS safety ranges based on thermal considerations. The current DBS safety guidelines are presumably solely based on charge delivery/electrochemical considerations. While waveforms with reversal of a stimulation phase (charge balanced stimulation) are advantageous from an electrochemical safety standpoint [44], they may be disadvantageous from a temperature safety standpoint (rms considerations). While lead/electrode selection does not necessarily factor in electrochemical safety considerations, thermal interaction between electrodes indicates that temperature-based safety guidelines must consider the electrode separation distance. Therefore, the design of DBS stimulation parameters to limit temperature increases should follow separate guidelines than those to limit charge delivery. Experimental validation and refinement of our basic model would help us to establish these guidelines.

One novel approach to mediating DBS-induced temperature increases, suggested by our simulations, is to increase the thermal conductivity of the insulating components of the leads.

Effects of physical properties of brain tissue, metabolism and blood perfusion on temperature increase

We examined two physical properties of the brain tissue: electrical conductivity and thermal conductivity; both factors affect the DBS-induced temperature distributions in the brain tissue. Electrical conductivity is a measure of how well a material accommodates the transport of electric charges. For a voltage-controlled source, increasing electrical conductivity increases the Joule heat (equation (1)) and hence the peak temperature. In contrast, increasing thermal conductivity increase enhances heat conduction away from the DBS electrode and decreases the peak temperature. Neither perturbation affected the temperature space constant; this is derived in the appendix.

In the present study we did not consider temperature-induced changes in electrical conductivity [3]; for the small changes in temperature induced by DBS, these changes would be presumably minor. We did not explicitly consider the electrode metal/electrolyte interface [44, 45].

Using electrodes 1 and 2 on Lead 3389 and the high stimulation setting (selected based on published clinical reports and stimulation guidelines) resulted in temperature increases of 0.35 to 0.82 °C in homogenous media; the consideration of lead physical properties or an encapsulation

layer would lower this amount. Because of limited parameterization data, we did not consider the effects of an imbalanced increase in metabolic and blood perfusion as a result of DBS; an increase in metabolic heat not fully compensated for by blood perfusion would further increase the brain temperature (in addition to DBS-induced Joule heating). In addition, we did not consider thermal tissue inhomogeneity or electrical inhomogeneity [35], outside the encapsulation layer; a combination of these could produce local DBS 'hot spots.'

Blood perfusion was modeled using the Penne model which has previously been applied in modeling ablative electrical stimulation of the brain [3, 47, 48]; in some of these reports simulation results were confirmed by *in vivo* experiments or clinical observation, suggesting that the Penne model provides a relatively accurate description of stimulation-induced temperature increases. More complex bio-heat models have been developed for muscles and kidney tissues [46, 54]; these models explicitly consider inhomogenous blood flow in these specific structures.

Brain metabolism and blood flow act in opposite directions in brain temperature regulation. Normally, the temperature of the blood going into the brain is lower than that in the brain tissue [33, 49], and blood flow thus acts as a heat sink. Electrical stimulation would be expected to increase metabolism by activating neurons and glia; this would synergistically act with electrical stimulation-induced Joule heat, while a regulatory increase in blood flow (vasodilatation) would counteract these changes. In this paper, metabolism and blood flow were balanced; this is not necessarily the case *in vivo*.

Functional implications

Sustained brain temperature increases above 40–41 °C may be considered as a threshold for pathological hyperthermia [49]. We did not observe increases to 40 °C under any conditions evaluated in the present report, suggesting that the specific stimulation settings tested will not directly lead to necrosis. The effect of the temperature increases observed in the present study (up to 0.8 °C) on tissue function strongly depends on the specific biophysical properties of the targeted tissue as well as the mechanisms by which deep brain stimulation electrically modifies tissue properties. The latter remains an area of active research. Changes of 1–2 °C can have significant effects on a single neuron and neuronal network function; the role of small temperature changes (<1 °C) has been less extensively tested. However, there is no threshold for temperature effects, such that any temperature increase will affect channel gating and pump kinetics. Moreover, sustained temperature increases over time will affect proliferation, excitability and connectivity [49]. Future studies controlling the temperature of acute brain slices [50, 51], including in combination with electrical stimulation [17, 24, 52], may directly address these mechanisms. The results of this prerequisite study provide the temperature ranges that should be evaluated. Future studies incorporating measurements of temperature changes in a bath system using Medtronic DBS leads and micro-thermal sensors may be used to validate the (no blood perfusion) predictions of the present study.

It is interesting to compare the spatial distribution of DBS-induced thermal fields with 'neuronal activation fields' predicted by previous computer simulation studies [45] and the spatial extent of blood perfusion increases shown by imaging studies [43]. The simulated neuronal activation fields and the temperature fields considered here are only coincidental of comparable orders. As noted above, we did not explicitly consider the effects of local neuronal activation on the temperature field. The temperature field may, in turn, affect the neuronal activation field through temperature-induced changes in the neuronal firing threshold. Increases in imaged brain–blood perfusion in response to DBS are also of a comparable spatial order, suggesting that they may represent a response to both increased neuronal activation and temperature increases.

Acknowledgments

We would like to thank Abhishek Datta and Thomas Radman for comments on an earlier version of this manuscript. This work was supported by Wallace Coulter, the Whitaker Foundation and a PSC-CUNY award.

Appendix

The temperature field around the DBS electrode is modeled as

$$\rho C_{\mathrm{p}} \frac{\partial T}{\partial t} = \nabla(k\nabla T) - \rho_{\mathrm{b}}\omega_{\mathrm{b}}C_{\mathrm{b}}(T - T_{\mathrm{b}}) + Q_{\mathrm{m}} + \sigma|\nabla V|^2. \tag{A.1}$$

At the steady state with constant thermal conductivity, κ, no perfusion rate ($\omega_{\mathrm{b}} = 0$) and no metabolic heat ($Q_{\mathrm{m}} = 0$), equation (A.1) is reduced to

$$\nabla^2 T = -\frac{\sigma}{K}|\nabla V|^2. \tag{A.2}$$

We applied cylindrical coordinates to equation (A.2) at a fixed plane $Z = 3$ mm (where peak temperature was observed). Therefore, the derivatives with respect to Z were equal to zero and the terms of ∇V and $\nabla^2 T$ were only the functions of variable r. Equation (A.2) is then reduced to

$$\frac{1}{r}\frac{\partial}{\partial r}\left(r\frac{\partial T}{\partial r}\right) = -\frac{\sigma}{K}|\nabla V|^2. \tag{A.3}$$

$$\frac{\partial}{\partial r}\left(r\frac{\partial T}{\partial r}\right) = -\frac{\sigma}{K}|\nabla V|^2 r. \tag{A.4}$$

Let $g(r) = |\nabla V|^2$

$$\left[r\frac{\partial T}{\partial r}\right]_{r_0}^{r} = -\frac{\sigma}{k}\int_{r_0}^{r} r g(r)\,\mathrm{d}r. \tag{A.5}$$

Let $f(r) = \int_{r_0}^{r} r g(r)\,\mathrm{d}r$

$$r\frac{\partial T}{\partial r} - r_0\left[\frac{\partial T}{\partial r}\right]_{r=r_0} = -\frac{\sigma}{k}f(r) \tag{A.6}$$

$$r\frac{\partial T}{\partial r} = -\frac{\sigma}{k}f(r) + r_0\left[\frac{\partial T}{\partial r}\right]_{r=r_0} \tag{A.7}$$

$$\frac{\partial T}{\partial r} = \frac{1}{r}\left(-\frac{\sigma}{k} f(r) + r_0 \left[\frac{\partial T}{\partial r}\right]_{r=r_0}\right). \tag{A.8}$$

When r_0 was chosen at the distant thermal boundary, the temperature at the thermal boundary, T_0, was 37 °C and the rate of temperature change approached zero. Hence, the derivative of temperature with respect to radius at the thermal boundary was zero, $\left[\frac{\partial T}{\partial r}\right]_{r=r_0} = 0$. So, equation (A.8) reduced to

$$\frac{\partial T}{\partial r} = -\frac{\sigma}{K}\frac{f(r)}{r} \tag{A.9}$$

$$T - T_0 = -\frac{\sigma}{k}\int_{r_0}^{r} \frac{f(r)}{r}\,\mathrm{d}r. \tag{A.10}$$

Let $h(r) = \int_{r_0}^{r} \frac{f(r)}{r}\,\mathrm{d}r$

$$T(r) = -\frac{\sigma}{k}h(r) + T_0. \tag{A.11}$$

As described above, $T_0 = 37$ °C

$$T(r) = -\frac{\sigma}{k}h(r) + 37 \tag{A.12}$$

$$T_{\text{peak}} = T_{r=r_{\text{P}}} = -\frac{\sigma}{k}h(r_{\text{P}}) + 37, \tag{A.13}$$

where r_{p} was fixed at the surface of electrodes on which peak temperature, T_{peak}, was observed. Note that the differential increase in temperature (T_{peak}—37), in homogenous tissue, is thus linearly related to tissue electrical conductivity and to the inverse of tissue thermal conductivity (this is confirmed in our numerical simulation table 1):

$$T_{\text{space}} = T_{r=r_{\text{s}}} = -\frac{\sigma}{k}h(r_{\text{s}}) + 37, \tag{A.14}$$

where r_{s} was defined as a temperature space constant:

$$\frac{T_{\text{space}} - 37}{T_{\text{peak}} - 37} = \frac{h(r_{\text{s}})}{h(r_{\text{p}})}. \tag{A.15}$$

At the temperature space constant, the temperature field decreased to 75% of its peak value at the electrode surface. Therefore, $\frac{T_{\text{space}}-37}{T_{\text{peak}}-37} = \frac{h(r_{\text{s}})}{h(r_{\text{p}})}$ was defined as 75%.

Changing either electrical conductivity (σ) or thermal conductivity (κ) will alter the peak temperature (T_{peak}) and the temperature at the distance of the space constant (T_{space}). However, the function $h(r)$ is independent of these tissue properties. So, the ratio of $h(r_s)$ to $h(r_p)$ is not a function of σ and κ. Therefore, the temperature space constant, $\frac{T_{\text{peak}}-37}{T_{\text{space}}-37} = \frac{h(r_{\text{p}})}{h(r_{\text{s}})}$, is not affected by σ and κ. It is important to note that the above analysis is not necessarily valid for inhomogenous conditions or in the presence of blood perfusion or metabolic heat.

References

[1] Tungjitusolmun S, Woo E J and Cao H 2000 Finite element analyses of uniform current density electrodes for radio-frequency cardiac ablation *IEEE Trans. Biomed. Eng.* **47** 32–40

[2] Labonte S 1994 Numerical model for radio-frequency ablation of the endocardium and its experimental validation *IEEE Trans. Biomed. Eng.* **41** 108–15

[3] Chang I 2003 Finite element analysis of hepatic radiofrequency ablation probes using temperature-dependent electrical conductivity *Biomed. Eng. Online* **2** 12

[4] LaManna J C, Rosenthal M, Novack R, Moffett D F and Jobsis F F 1980 Temperature coefficients for the oxidative metabolic responses to electrical stimulation in cerebral cortex *J. Neurochem.* **34** 203–9

[5] LaManna J C, McCracken K A, Patil M and Prohaska O J 1988 Brain tissue temperature: activation-induced changes determined with a new multisensor probe *Exp. Med. Biol.* **222** 383–9

[6] LaManna J C, McCracken K A, Patil M and Prohaska O J 1989 Stimulus-activated changes in brain tissue temperature in the anesthetized rat *Metab. Brain Dis.* **4** 225–37

[7] Tasaki I and Byrne P M 1987 Heat production associated with synaptic transmission in the bullfrog spinal cord *Brain Res.* **407** 386–9

[8] Hoffmann H M and Dionne V E 1983 Temperature dependence of ion permeation at the endplate channel *J. Gen. Physiol.* **81** 687–703

[9] Moser E, Mathiesen I and Andersen P 1993 Association between brain temperature and dentate field potentials in exploring and swimming rats *Science* **259** 1324–6

[10] Stiles J R, Kovyazina I V, Salpeter E E and Salpeter M M 1999 The temperature sensitivity of miniature endplate currents is mostly governed by channel gating: evidence from optimized recordings and Monte Carlo simulations *Biophys. J.* **77** 1177–87

[11] Bennetts B, Roberts M L, Bretag A H and Rychkov G Y 2001 Temperature dependence of human muscle ClC-1 chloride channel *J. Physiol.* **535** 83–93

[12] Fujii S, Sasaki H, Ito K, Kaneko K and Kato H 2002 Temperature dependence of synaptic responses in guinea pig hippocampal CA1 neurons *in vitro Cell Mol. Neurobiol.* **22** 379–91

[13] Collins C A and Rojas E 1982 Temperature dependence of the sodium channel gating kinetics in the node of Ranvier *Q. J. Exp. Physiol.* **67** 41–55

[14] Dostrovsky J O, Levy R, Wu J P, Hutchison W D, Tasker R R and Lozano A M 2000 Microstimulation-induced inhibition of neuronal firing in human globus pallidus *J. Neurophysiol.* **84** 570–4

[15] Pierau F R, Klee M R and Klussmann F W 1976 Effect of temperature on postsynaptic potentials of cat spinal motoneurones *Brain Res.* **114** 21–34

[16] Bikson M, Lian J, Hahn P J, Stacey W C, Sciortino C and Durand D M 2001 Suppression of epileptiform activity by high frequency sinusoidal fields in rat hippocampal slices *J. Physiol.* **531** 181–91

[17] Lian J, Bikson M, Sciortino C, Stacey W C and Durand D M 2003 Local suppression of epileptiform activity by electrical stimulation in rat hippocampus *in vitro J. Physiol.* **547** 427–34

[18] Lewis D V and Schuette W H 1975 Temperature dependence of potassium clearance in the central nervous system *Brain Res.* **99** 175–8

[19] Lothman E, Lamanna J, Cordingley G, Rosenthal M and Somjen G 1975 Responses of electrical potential, potassium levels, and oxidative metabolic activity of the cerebral neocortex of cats *Brain Res.* **88** 15–36

[20] Windels F, Bruet N, Poupard A, Urbain N, Chouvet G, Feuerstein C and Savasta M 2000 Effects of high frequency stimulation of subthalamic nucleus on extracellular glutamate and GABA in substantia nigra and globus pallidus in the normal rat *Eur. J. Neurosci.* **12** 4141–6

[21] Bruet N, Windels F, Bertrand A, Feuerstein C, Poupard A and Savasta M 2001 High frequency stimulation of the subthalamic nucleus increases the extracellular contents of

striatal dopamine in normal and partially dopaminergic denervated rats *J. Neuropathol. Exp. Neurol.* **60** 15–24
[22] Savasta M, Windels F, Bruet N, Bertrand A and Poupard A 2002 Neurochemical modifications induced by high-frequency stimulation of subthalamic nucleus in rats *The Basal Ganglia VII* ed Nicholsson L (Dordrecht: Kluwer) pp 581–90
[23] Urbano F J, Leznik E and Llinas R R 2002 Cortical activation patterns evoked by afferent axons stimuli at different frequencies: an in vitro voltage-sensitive dye imaging study *Thalamus Rel. Syst.* **1** 371–8
[24] Lee K H, Chang S Y, Roberts D W and Kim U 2004 Neurotransmitter release from high-frequency stimulation of the subthalamic nucleus *J. Neurosurg.* **101** 511–7
[25] Abbott B C, Howarth J V and Ritchie J M 1965 The initial heat production associated with the nerve impulse in crustacean and mammalian non-myelinated nerve fibres *J. Physiol.* **178** 368–83
[26] Rezai A R, Lozano A M, Crawley A P, Joy M L, Davis K D, Kwan C L, Dostrovsky J O, Tasker R R and Mikulis D J 1999 Thalamic stimulation and functional magnetic resonance imaging: localization of cortical and subcortical activation with implanted electrodes. *Technical note J. Neurosurg.* **90** 583–90
[27] Zonenshayn M, Mogilner A Y and Rezai A R 2000 Neurostimulation and functional brain imaging *Neurol. Res.* **22** 318–25
[28] McIntyre C C, Savasta M, Kerkerian L, Goff L and Vitek J L 2004 Uncovering the mechanism(s) of action of deep brain stimulation: activation, inhibition, or both *Clin. Neurophysiol.* **115** 1239–48
[29] Fiala D, Lomas K J and Stohrer M 1999 A computer model of human thermoregulation for a wide range of environmental conditions: the passive system *J. Appl. Physiol.* **87** 1957–72
[30] Duck F A 1990 *Physical Properties of Tissues: A Comprehensive Reference Book* (San Diego: Academic)
[31] Implant Manual. *Medtronic 3387,3389 Lead Kit for Deep Brain Stimulation* 2003
[32] Baysal U and Haueisen J 2004 Use of *a priori* information in estimating tissue resistivities-application to human data *in vivo Physiol. Meas.* **25** 737–48
[33] Collins C, Smith M and Turner R 2004 Model of local temperature changes in brain upon functional activation *J. Appl. Physiol.* **97** 2051–5
[34] Xiaojiang X, Tikuisis P and Giesbrecht G 1999 A mathematical model for human brain cooling during cold-water near-drowning *J. Appl. Physiol.* **86** 265–72
[35] McIntyre C, Mori S, Sherman D, Thakor N and Vitek J 2004 Electric field and simulating influence generated by deep brain stimulation of the subthalamic nucleus *Clin. Neurophysiol.* **115** 589–95
[36] Steffens H J and Prescott J 1979 *Joule and Concept of Energy* (New York: Science History Publications)
[37] Beurrier C, Bioulac B, Audin J and Hammond C 2001 High-frequency stimulation produces a transient blockade of voltage-gated currents in subthalamic neurons *J. Neurophysiol.* **85** 1351–6
[38] Cengel, Yunus A, Turner and Robert H 2004 *Fundamentals of Thermal-Fluid Sciences* (New York: McGraw-Hill) Science Pub Date: 2004–03-30
[39] Goodfellow Corporation (DEVON, PA) *Material Properties* http://www.goodfellow.com/csp/active/gfHome.csp
[40] Wei F X and Grill W M 2005 Current density distributions, field distributions and impedance analysis of segmented deep brain stimulation electrodes *J. Neural. Eng.* **2** 139–47
[41] Lide David R 2001 *Handbook of Chemistry and Physics* 81st edition (Boca Raton, FL: CRC Press)
[42] Tungjitkusolmun S, Staelin S Tyler, Haemmerich D, Tsai J Z, Cao H, Webster J G and Vorperian V R 2002 Three-dimensional finite-element analyses for radio-frequency hepatic tumor ablation *IEEE Trans. Biomed. Eng.* **49** 3–9
[43] Perlmutter J S, Mink J W, Bastian A J, Zackowski K, Hershy T, Miyawaki E, Koller W and Videen T O 2002 Blood flow responses to deep brain stimulation of thalamus *Neurology* **58** 1388–94
[44] Merrill D R, Bikson M and Jefferys J G 2005 Electrical stimulation of excitable tissue design of efficacious and safe protocols *J. Neurosci. Methods* **141** 171–98
[45] Christophor R B and McIntyre C 2005 Tissue and electrode capacitance reduce neural activation volumes during deep brain stimulation *Clin. Neurophysiol.* **116** 2490–500
[46] Arkin H, Xu L X and Holmes K R 1994 Recent developments in modeling heat transfer in blood perfused tissues *IEEE Trans. Biomed. Eng.* **41** 97–107
[47] Nelson D A, Nelson M T, Walters T J and Mason P A 2000 Skin heating effects of millimeter wave irradiation thermal modeling results *IEEE Trans. Microw. Theory Tech.* **48** 2111–20
[48] DeMarco S C, Lazzi G, Liu W, Weiland J D and Humayun Mark S 2003 Computed SAR and thermal elevation in a 0.25 mm 2-D model of the human eye and head in response to an implanted retinal stimulator *IEEE Trans. Antennas Propag.* **51** 2274–85
[49] Kiyatkin E A 2004 Brain hyperthermia uring physiological and pathological conditions: causes mechanisms, and functional implications *Curr. Neurovascular Res.* **1** 77–90
[50] Thompson S M, Masukawa L M and Prince D A 1985 Temperature dependence of intrinsic membrane properties and synaptic potentials in hippocampal CA1 neurons *in vitro J. Neurosci.* **5** 817–24
[51] Schiff S J and Somjen G G 1985 The effects of temperature on synaptic transmission in hippocampal tissue slices *Brain Res.* **345** 279–84
[52] Anderson T, Hu B, Pittman Q and Kiss Z H T 2004 Mechanisms of deep brain stimulation: an intracellular study in rat thalamus *J. Physiol.* **559** 301–13
[53] Astron M, Johansson J D, Hariz M I, Eriksson O and Wardell K 2006 The effect of cystic cavities on deep brain stimulation in the basal ganglia: a simulation-based study *J. Neural. Eng.* **3** 132–8
[54] Wren J, Karlsson M and Loyd D 2001 A hybrid equation for simulation of perfused tissue during thermal treatment *Int. J. Hyperth.* **17** 483–98
[55] Kiyatkin E A and Mitchum R 2003 Fluctuations in brain temperatures during sexual behavior in male rats: an approach for evaluating neural activity underlying motivated behavior *Neuroscience* **119** 1169–83
[56] Kiyatkin E A and Wise R A 2001 Striatal hyperthermia associated with arousal: intracranial thermorecordings in behaving rats *Brain Res.* **918** 141–52
[57] Cheuvront S N and Haymes E M 2001 Thermoregulation and marathon running: biological and environmental influences *Sports Med.* **31** 743–62
[58] Sharma H S and Hoopes P J 2003 Hyperthermia-induced pathophysiology of the centeral nervous system *Int. J. Hyperth.* **19** 325–54
[59] Kainz W, Neubauer G, Uberbacher R, Alesch F and Chan D D 2002 Temperature measurement on neurological pulse generators during MR scans *Biomed. Eng. Online* **1**:2
[60] Golombeck M A, Thiele J and Dossel O 2002 Magnetic resonance imaging with implanted neurostimulators: numerical calculation of the induced heating *Biomed. Tech. (Berl.)* **47** Suppl. 1 660–3